Design and Characterization of a Combined Low Power Voltage and Current Instrument Transformer for Low Voltage Applications

Youpeng Huangfu, *Member, IEEE*, Marco Faifer, *Senior Member, IEEE*, Roberto Ottoboni, *Fellow, IEEE*, and Sergio Toscani, *Senior Member, IEEE*

***Abstract*—Recent trends in smart substations have massively motivated the integration of low power instrument transformers for the purpose of metering, monitoring, protection and control. In this paper, a novel design principle for the development of a combined low power voltage and current instrument transformer for low voltage applications is proposed. In specific, a capacitive voltage divider and a shielded Rogowski coil are employed for voltage and current measurement, respectively. Interestingly, the Rogowski coil shield is exploited as an electrode for the high voltage capacitance of the voltage divider. A prototype featuring the rated primary voltage of 400V and the rated primary current of 500A has been developed. Subsequently, basic accuracy characterization studies have been carried out. Experimental results confirm the full compliance of the combined transducer with IEC 61869 standards, assuring 0.5 and 0.1 accuracy classes for voltage and current measurement, respectively. This research provides a compact and cost-effective solution for combined low voltage low power instrument transformers with high precision and wide dynamic range.**

***Index Terms*—Capacitive voltage divider, low power instrument transformer, smart substations, Rogowski coil.**

I. Introduction

DRIVEN by the evolution of smart substations, non-conventional low power instrument transformers (LPITs) have been experiencing extensive deployment in the distribution networks in medium voltage (MV) and high voltage (HV) applications [1]-[3]. By definition, voltage and current LPITs convert high voltage and current to standardized low and easily measurable signals for multi-purpose utilizations, for instance, metering, monitoring, protection and control. In general, in comparison to the induction transformers, both low power voltage transformers (LPVTs) and low power current transformers (LPCTs) feature advantages in terms of dimensions, weight, reliability, and safety due to the absence of saturation and ferro-resonance phenomena [4], [5]. In recent years, standardization work included in IEC 61869 series has been progressively carried out for the definition of general requirements of LPVTs [6] and LPCTs [7] in different operating conditions, both normal and special applications [8]. Furthermore, owing to the improvement of digitalized substations and intelligent electronic devices (IEDs), considerable research efforts have been triggered in order to design and develop more innovative solutions for LPITs with high accuracy and reliability.

For voltage measurement in most MV and HV networks, LPVTs are designed based on the principle of a resistive [9], [10] or a capacitive voltage divider scheme [11]-[13]. Straightforwardly, either method generates an output voltage signal which is directly proportional to the primary voltage to be measured. Generally, a capacitive voltage divider is implemented by coaxial electrodes. To fulfil optimal designs of LPVTs, mathematical modeling research and characterization study have been conducted, with a specific attention to the evaluations of the influence of proximity effect [14], of temperature and frequency [15], and of external electric fields [16]. Additionally, for the purpose of accuracy assessment, plenty fundamental discussions on the calibration approach [17] and uncertainty quantification analysis [18]-[21] have been actively performed.

For the purpose of current measurement, Rogowski coils (RCs) based LPCTs have been proved to be a popular solution. Specifically, the RC type LPCT is an air-core current transducer working on the fundamental principles of Ampere's and Faraday's law [22]-[24]. The output voltage signal of an RC is a scaled time derivative of the primary current to be measured. This low amplitude voltage signal can then be processed and integrated by using the connected IEDs. As a matter of fact, the accuracy of the RC based LPCT is dominated by the mutual inductance between the primary conductor and the RCs. For this reason, the critical parameters that affect the mutual inductance in terms of the number of turns with uniform or non-uniform windings [25], skeleton structures [26] as well as the positioning issues [27]-[29] have to be characterized. Another important requirement for MV and HV LPCTs is the capability

This work was supported in part by the State Key Laboratory of Electrical Insulation and Power Equipment (EIPE24208), Xi'an Jiaotong University, China.

Youpeng Huangfu is with the State Key Laboratory of Electrical Insulation and Power Equipment, School of Electrical Engineering, Xi'an Jiaotong University, Xi'an 710049, China. (youpeng.huangfu@xjtu.edu.cn, youpeng.huangfu@polimi.it)

Marco Faifer, Roberto Ottoboni, and Sergio Toscani are with the Department of Electronics, Information and Bioengineering, Politecnico di Milano, Milan 20133, Italy. (marco.faifer@polimi.it, roberto.ottoboni@polimi.it, sergio.toscani@polimi.it).

to reject interferences due to the external magnetic fields especially in a very compact switchgear environment. To this purpose, a magnetic shielding schematic is usually adopted [30]. Some previous works demonstrate the superior magnetic shielding effectiveness in RCs [31], [32], enabling high levels of accuracy of current measurement.

In addition to individual LPVTs and LPCTs, combined voltage and current LPITs are good options especially for modern smart substations with space constraints. By definition, a combined LPIT essentially comes integrating voltage and current measurement into a single unit. Such an integration is able to cover a wide range of applications, providing a safe, reliable, and standardized solution for LPITs. In [33] and [34], combined electronic voltage and current transformers with different construction structures are proposed. Nevertheless, they are basically adopting the same principles for the voltage and current measurements, that is, a capacitive divider for voltage measurement and an RC for current transfer. In [35], an unconventional combined instrument transformer is studied, where the capacitors of the voltage transformer and coils of the current-to-voltage transducers are designed based on printed circuit board technology. In [36] and [37], a floating conductor is employed at the gas insulated substations enclosure, serving as a sensing electrode in the capacitive voltage divider. As known, critical problems in terms of dielectric insulation and surface discharges appear in the MV and HV combined transformers. Thereby, electric stress analysis typically has to be conducted, as demonstrated in [35] and [38].

As discussed above, combined LPITs are generally applied in MV and HV distribution networks up to now while in low voltage (LV) applications traditional bulky CTs and VTs are still commonly used. As a matter of fact, this LPIT technology also lends itself to interesting utilizations in LV power networks. In this case, lower insulation requirement makes it possible to develop smaller, smarter as well as more cost-effective solutions for LPITs. To this purpose, this paper proposes an innovative structure for combined LPITs with specific applications in LV networks, assuring reliable insulation. The purpose of the proposed combined LPIT is to replace the traditional CTs and VTs in LV applications. Essentially, in this proposed combined LPIT structure, a shielded RC with a nonmagnetic core is used for the current measurement. In addition, to fulfil the voltage measurement purpose, a capacitive divider is constructed with the aid of the stray capacitance between the primary conductor and the RC shield and the adoption of a physical capacitor. Remarkably, the RC shield is exploited as a sensing electrode for the high voltage capacitance of the voltage divider, and therefore, no additional sensing electrode is required in this proposed structure, yielding a simple and compact implementation. In short, this new construction features the proven measurement principles of RC for current measurement and capacitive divider for voltage transfer, respectively. Furthermore, standardized low and easily measurable voltage signals both for voltage and current measurements are enabled by assembling individual front-end low power conditioning circuits.

This novel conception blends the traditional and advanced technologies thus permits the new generation of combined LV LPIT to be able to achieve a compact and cost-effective solution, and significantly preserving high accuracy and reliability. Following the aforementioned basic principles, a combined LV LPIT prototype is developed and is then subjected to experimental tests in order to prove the compliance with specified accuracy class defined in currently applicable standards.

The remainder of this paper is structured as follows. The fundamental principles of voltage and current measurements for the combined LPIT are demonstrated in Section II. Driven by the basic architecture, a combined LPIT prototype is developed as a result in Section III. Section IV devotes to the experimental characterization study of the combined LPIT prototype from the perspective of amplitude and frequency linearities. General conclusions are drawn in Section V.

II. Fundamental Principles of the Proposed Combined LV LPIT

In this Section, the fundamental design principles of the proposed combined LPIT construction will be presented. As mentioned, the measurement principle of the combined LPIT is based on a capacitive divider for voltage transduction and a shielded RC for current measurement. In specific, the proposed construction of the combined LPIT unit is simply composed of a cuboidal metallic enclosure, accommodating a proper resin insulating material, and a non-magnetic shielded RC. The shielded RC is situated at the center of the cuboidal enclosure.

A cross-section view of the LPTI geometry is depicted in Fig. 1. As shown in the diagram, both the capacitive voltage divider and the shielded RC are integrated into the metallic enclosure. As indicated, the enclosure is directly shorted to the reference ground, providing robust shielding and zero potential. Note that an appropriate resin is employed to bridge the gap between the primary conductor (busbar) and the RC shield.

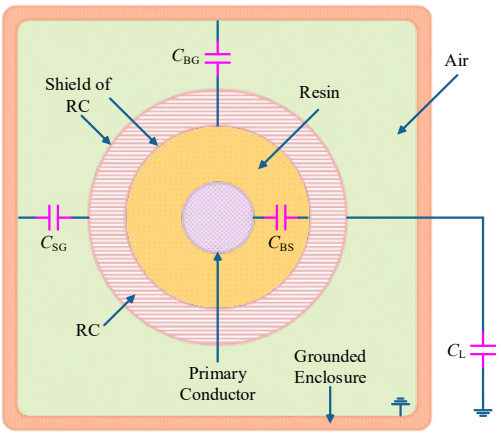

Fig. 1. A cross-section view of the geometry diagram of the proposed combined LV LPIT construction.

The high-voltage capacitor of the voltage divider is ideally formed by the stray capacitance C_{BS} between the busbar and the RC shield. Importantly, a physical capacitor C_L connected

between the RC shield and the ground terminal performs the low voltage capacitor of the divider. Remark that C_{BG} and C_{SG} are the stray capacitances between the primary busbar and the grounded enclosure, and between the RC shield and the enclosure, respectively. As is well known, due to the frequency dependent and temperature drift phenomena, nonlinear behavior of the relative conductivity and permittivity of a resin material will be inevitably introduced. As a consequence, in order to mitigate the influence of stray capacitances and stray resistances on the accuracy of the capacitive voltage divider and considering the LV applications, air insulation is adopted between the RC shield and the enclosure.

A. Capacitive Voltage Divider of the Combined LPIT

Typically, a basic capacitive voltage divider consists of two capacitors, where the divider ratio is dominated by the ratio of the two capacitance values. Nevertheless, in practical designs, as indicated in Fig. 1, the ratio of the capacitive voltage divider will be unavoidably influenced by other stray capacitances involved in the construction. In addition, another aspect that should be considered is the stray resistances introduced by the adoption of the resin material. However, the stray resistance values, in general, compared with the reactance of the involved capacitances, are negligible. As a consequence, a more realistic while still significantly simplified equivalent circuit model of the capacitive voltage transducer is illustrated in Fig. 2. As can be noted, $U_P(t)$ and $U_S(t)$ are the primary and secondary voltages, respectively. In addition, R is a termination resistor typically with a high value.

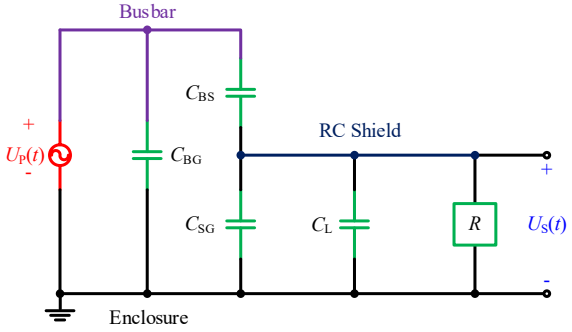

Fig. 2. Equivalent circuit model for the capacitive voltage divider of the combined LPIT.

With respect to the equivalent circuit in Fig. 2, the transfer function of the capacitive voltage divider can be derived. In Fourier domain, it can be expressed as

$$\frac{U_P(j\omega)}{U_S(j\omega)} = \frac{\frac{1}{R} + j\omega(C_{BS} + C_{SG} + C_L)}{j\omega C_{BS}} \tag{1}$$

where, ω is the angular frequency. Under the condition that

$$\frac{1}{R} \ll \omega(C_{BS} + C_{SG} + C_L) \tag{2}$$

(1) can be further simplified to be.

$$\frac{U_P(j\omega)}{U_S(j\omega)} \approx \frac{C_{BS} + C_{SG} + C_L}{C_{BS}} \tag{3}$$

As indicated in (3), by measuring the voltage signal U_S, the primary voltage to be measured U_P can then be evaluated. What is noteworthy is that the voltage ratio is actually dominated by C_{BS} and the summation of C_{BS}, C_{SG}, and C_L. In fact, the value of the stray capacitance C_{BS} is determined by the geometry and the employed dielectric material. In general, the stray capacitances are very small and are at the level of pF. In practical applications, to adapt the primary voltage U_P to be measured to the levels compatible with a data acquisition (DAQ) board, the capacitance value of the physical capacitor C_L should be appropriately selected.

To guarantee a good accuracy of the voltage divider, the value of C_{BS} must be as stable as possible over temperature and over frequency. Consequently, an appropriate resin between the busbar and the RC shield which has a constant relative permittivity versus both temperature and frequency is mandatory. For the same reasons, the same characteristics must be also assured for the physical capacitor C_L.

B. Shielded RC Based Current Transformer of the Combined LPIT

The introduction of RC based current measurement principle is a typical paradigm shift in the field of advanced technology. To assure good linearity and no saturation effect, the RCs must be wound uniformly over a stand-alone non-magnetic skeleton, instead of over an iron core used in an inductive current transformer. As a consequence, an RC is designed so that the primary and secondary windings are weakly coupled. High quality RC features a mutual inductance between the primary and secondary windings fairly constant for any position of the busbar inside the coil loop. Moreover, to guarantee the stability of this parameter the busbar and the RC are usually blocked from each other. Furthermore, a shield is mandatory to prevent nuisance interference from nearby conductors carrying high currents.

Fig. 3 shows a simplified schematic of a shielded RC. It provides an induced output voltage $e(t)$ which represents the alternating primary current $I_P(t)$.

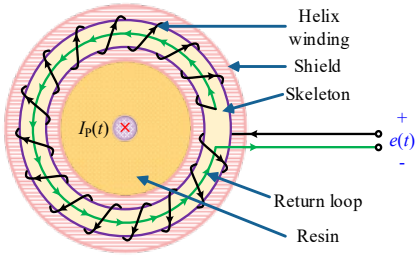

Fig. 3. Simplified sketch of a shielded RC.

Suppose the current carrying primary conductor being measured is long and straight. Referring to Fig. 3 and according to the Faraday's Law, the induced voltage $e(t)$ on the two output terminals of the RC can then be written as the following governing equation:

$$e(t) = -M\frac{dI_P(t)}{dt} \tag{4}$$

where M is the mutual inductance between the primary conductor and the RC.

A signal conditioning circuit is in general required in order to extract and process the RC output for further applications. For achieving high accuracy, the output of the RC shall be connected to electronics having a sufficiently high input impedance, resulting in a negligible current flowing through the secondary circuit. Generally, the RC output $e(t)$ is in the order of millivolts at rated primary current and rated frequency. Therefore, proper amplification has to be introduced to adapt the signal to the input range of ADCs.

III. Architecture of the Developed Combined LPIT Prototype

In this Section, the developed combined LPIT prototype with rated primary voltage of 400V and rated primary current of 500A with rated frequency of 50Hz is described. Fig. 4 and TABLE I illustrate the longitudinal section view of the geometry diagram and the dimensions of the prototype, respectively. Can be noted that an RC skeleton having a rectangular section is used. Prior to the prototype, the insulation performance of the LPIT is validated by using an electrostatic finite element method (FEM).

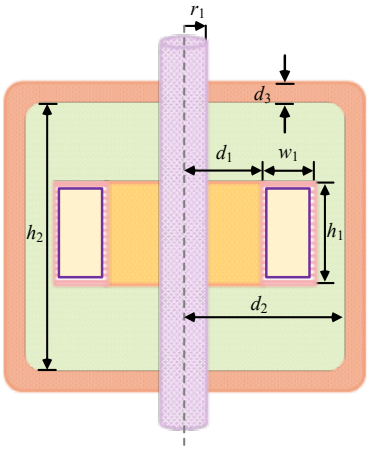

Fig. 4. Longitudinal section view of the developed combined LPIT prototype.

TABLE I. Dimensions of the combined LPIT prototype.

Item	Value (mm)	Item	Value (mm)
d_1	28	r_1	20
d_2	47	h_1	28
d_3	3	h_2	75
w_1	11		

To guarantee high accuracy of the capacitive voltage divider scheme, an acetal homopolymer resin with an outstanding balance of electrical and thermal properties is employed to bridge the gap between the busbar and the RC shield. Moreover, it offers superior electrical insulation property and a low thermal expansion rate.

The stray capacitances in the capacitive voltage divider have been numerically computed by the electrostatic FEM. Having the values of the stray capacitances, an appropriate value of the physical capacitor C_L can then be determined, in order to assure the maximum output voltage of the voltage channel to a suitable value to be acquired. The primary aim of this choice is to generate an appropriate output voltage level for the characterization study of the prototype.

Through the same FEM analysis, the effect of possible misalignment of the position of the primary conductor with respect to RC has been estimated. The analysis pointed out that the displacement up to 1 mm has results in variation up to 0.64% of divider ratio coefficient, keeping constant CL.

This error can be considered as a systematic error (the geometry of the system cannot change anymore once the LPVT has been built), and it can be removed by the final calibration. It is important to notice that the calibration is always required when high accuracy classes is targeted.

For a feasible measurement purpose by using a DAQ board, a front-end circuit for the voltage channel is designed to replace the termination resistor R as illustrated in Fig. 2. The schematic is presented in Fig. 5 (a), providing an output voltage $U_{S,u}(t)$. It integrates a termination resistor R_L and an operational amplifier (OPA) with a unity gain. Remark that the R_L function is to limit the effect of the input bias current of the OPA, avoiding its saturation. In this paper, a low cost, high speed as well as precision monolithic OPA AD711JR is employed to achieve superior low offset voltage. Importantly, in order to fulfil the condition as required in (2) and assuring, at the same time, a low offset output voltage, a value of 100MΩ is selected for R_L.

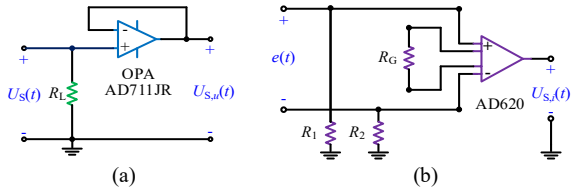

Fig. 5. Schematics of the front-end circuit for (a) the capacitive voltage divider and (b) the RC based current transformer.

As far as the current channel is concerned, a shielded RC which is specifically designed in a rated ratio of 500A/150mV at rated frequency of 50Hz is employed. The front-end conditioning circuit of the current channel is presented in Fig. 5 (b). In this paper, a low cost, low power, and high accuracy instrumentation amplifier AD620, is employed. In addition, R_1 and R_2 are two identical common mode input resistors.

With respect to Fig. 5 (b), the relation between the output of the conditioning circuit $U_{S,i}(t)$ and the RC output $e(t)$ yields

$$U_{S,i}(t) = G \cdot e(t) \tag{5}$$

where G is the gain of the conditioning circuit.

According to the aforementioned criteria, a front-end circuit board featuring both voltage and current channels has been implemented. Moreover, a metallic envelope is employed in order to improve the immunity behavior of the circuit board to external electromagnetic interferences. A DAQ board has been used to convert the output analog voltage signals from the voltage and current channels of the combined LPIT to digital ones for further characterization study. In addition to high speed and excellent noise performance, all the adopted IEDs are characterized by high linearity and extremely low temperature drift, over a wide temperature range and frequency bandwidth.

IV. Characterization of the Combined LPIT Prototype

This Section reports the characterization study of the developed combined LPIT prototype. More specifically, experimental tests have been performed in terms of amplitude and frequency linearities.

A. Characterization Procedure and Measurement Setup

As a first step, a principal characterization procedure has been designed for basic accuracy tests. To this end, the measurement setup schematized in Fig. 6 has been implemented.

To characterize the capacitive voltage divider unit, a FLUKE 5502E multifunction calibrator is employed, as illustrated in Fig. 6. It provides a high precision sinusoidal voltage source, with a maximum voltage up to 1020V in a wide frequency bandwidth. An active differential probe, CT4066 with accuracy class 0.2, has been used as voltage reference. This probe has been calibrated by means of the calibrator FLUKE 5502E and a Fluke 8508 multimeter in the voltage and frequency ranges of interest. The resulting relative uncertainty has been estimated to be lower 0.1% (with cover factor k=2). A phase meter Powertek SD1000 has been used to evaluate the phase uncertainty. It has been determined that the transducer phase uncertainty is better than 0.07 crad at frequencies lower then 1kHz and better than 0.12crad in the frequency range 1 kHz to 5 kHz (k=2). As current reference, an electronic current transducer LEM IN 500-S with an accuracy of 0.0018% has been employed, providing very high accuracy and excellent linearity in a wide frequency bandwidth. The output of the current transducer is connected to a reference shunt resistor giving an overall uncertainty of 0.05% (k=2). In addition, a multifunction NI USB-6356 DAQ is adopted to acquire the voltage signals from the reference systems and from the combined LPIT prototype. It offers 16-bit resolution, input voltage range ±10V, and maximum sampling frequency 1.25MS/s.

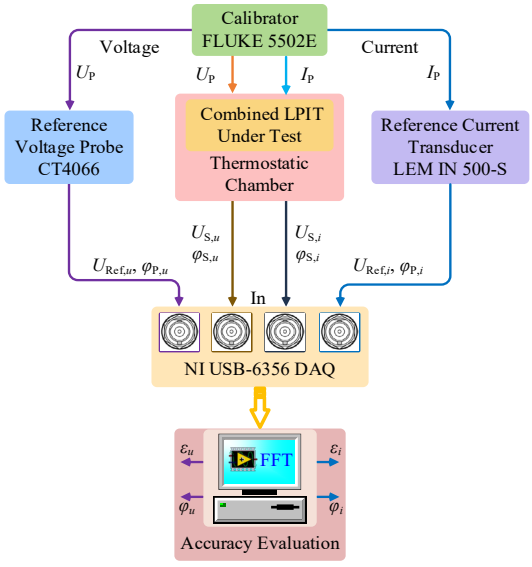

Fig. 6. Principal diagram for accuracy test of the combined LPIT prototype.

For the evaluation of the influence of temperature variation, as can be noted from Fig. 6, a thermostatic chamber is used to host the combined LPIT prototype.

The calibrator FLUKE 5502E can only generate a maximum current up to 20.5A. This current source is used for the temperature cycle accuracy test, as shown in the schematic in Fig. 6. An additional accuracy test at rated current has been conducted by extending the current source range up to 500A. This test circuit basically is implemented by adopting a power amplifier and a step-up current transformer. For brevity, the test schematic and measurement setups are shown in Fig. 7 (a) and (b), respectively. The power amplifier is fed with a sinusoidal signal synthesized by an NI 6356 DAQ board.

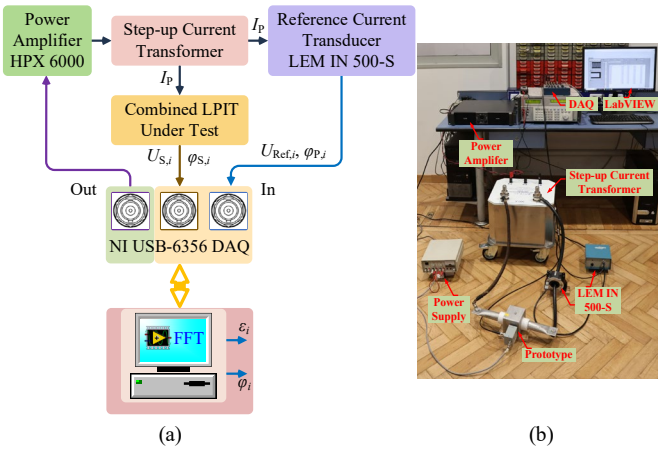

(a) (b)

Fig. 7. (a) Test schematic and (b) measurement setup for the current channel of the combined LPIT at rated current.

As indicated in Fig. 6, the voltage/current (referred to as RMS U_P and I_P) generated by the calibrator is simultaneously applied both to the reference voltage/current reference transducer and to the combined LPIT prototype under test. The measurement process implies comparisons of the signals obtained from the reference transformers and from the LPIT prototype. As a consequence, the ratio errors and phase displacements of the LPIT prototype under test can be determined on the basis of comparison results. In accordance with Fig. 6, the percentual ratio error for voltage (ε_u) or current (ε_i) and the phase displacement for voltage (φ_u) or current (φ_i) are defined by the following formulae:

$$\begin{cases} \varepsilon_u = \dfrac{K_{r,u}U_{S,u} - U_P}{U_P} \times 100 \\ \varphi_u = \varphi_{S,u} - \varphi_{P,u} \end{cases} \tag{6}$$

$$\begin{cases} \varepsilon_i = \dfrac{K_{r,i}U_{S,i} - I_P}{I_P} \times 100 \\ \varphi_i = \varphi_{S,i} - \varphi_{P,i} \end{cases} \tag{7}$$

where, $K_{r,u}$ and $K_{r,i}$ are the rated voltage and current transformation ratios at rated frequency of 50Hz, respectively. Additionally, $U_{S,u}$ and $U_{S,i}$ are the RMS secondary output signals of the voltage and current channels, respectively; $\varphi_{P,u}$ and $\varphi_{S,u}$ are the phase angles of the primary and secondary voltages of the voltage channel, respectively; $\varphi_{P,i}$ and $\varphi_{S,i}$ are the

phase angles of the primary current and secondary voltage of the current channel, respectively.

It must be underlined that, from the standard point of view, the above definitions in (6) and (7) are strictly correct only for sinusoidal voltages and currents. As a consequence, specific care must be taken to compute the ratio errors and phase displacements. In this paper, the Fast Fourier Transform (FFT) implemented in the LabVIEW program is applied in order to extract the spectral component of the measured signals at a given frequency of interest.

Note that the following characterization studies are carried out at a constant room temperature of 25°C unless otherwise specified.

B. Characterization of the Capacitive Voltage Divider of the Combined LPIT Prototype

The primary measurement purpose to the capacitive voltage divider is to prove compliance with the specified measuring accuracy class. A preliminary calibration of the LPIT has been performed at the frequency of 50Hz, both for voltage and current channels, operating at the rated input values.

Then measurements are performed at considered percentages of rated voltage 80%, 100%, and 120%, in the rated frequency range from 99% to 101%, that is, 49.5Hz, 50Hz, and 50.5Hz. Note that 40 repetitive tests are carried out for each scenario. The rated ratio of the capacitive divider is evaluated by means of the average of 40 test samples at rated primary voltage 400V and at rated frequency 50Hz. The distributions of ratio error and phase displacement at each specific frequency are illustrated in Fig. 8 (a), (b), and (c).

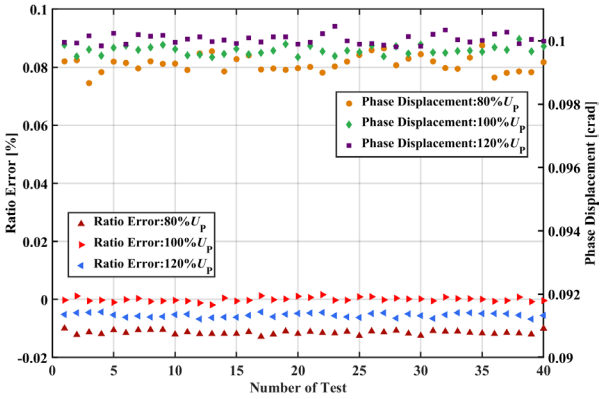

(a)

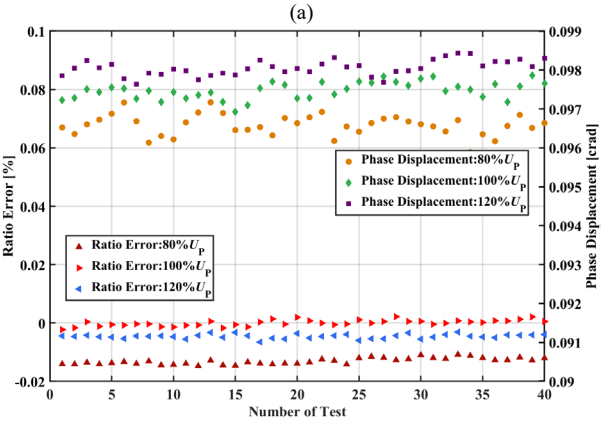

(b)

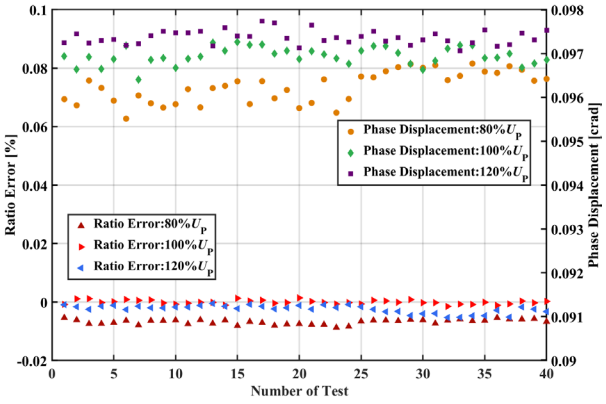

(c)

Fig. 8. Distributions of ratio error and phase displacement at 80%U_P, 100%U_P, and 120%U_P at (a) 49.5Hz, (b) 50Hz, and (c) 50.5Hz.

To quantify the dispersion performance of the observations, the Type-A standard uncertainties for the ratio error ($u_A(\bar{\varepsilon}_u)$) and phase displacement ($u_A(\bar{\varphi}_u)$) are evaluated by (8):

$$u_A(\mu)=\sqrt{\frac{\sum_{n=1}^{N}(x_n-\mu)^2}{N(N-1)}} \tag{8}$$

where μ represents the mean value of ratio error $\bar{\varepsilon}_u$ or phase displacement $\bar{\varphi}_u$; x_n denotes the measurement result of ratio error or phase displacement; N is the total number of the repetitive test.

As a result, the mean values and the Type-A standard uncertainties are listed in TABLE II. As can be noted, the results clearly demonstrate the high accuracy and stability of the capacitive voltage divider unit.

TABLE II. Mean values and Type-A standard uncertainties of ratio error and phase displacement of the voltage divider at 49.5Hz, 50Hz, and 50.5Hz.

Percentage of U_P [%]	Parameter	Item	Frequency [Hz]		
			49.5	50	50.5
80	Ratio error	$\bar{\varepsilon}_u$ [%]	-0.011	-0.013	-0.007
		$u_A(\bar{\varepsilon}_u)$	1.1×10^{-4}	1.7×10^{-4}	1.3×10^{-4}
	Phase displacement	$\bar{\varphi}_u$ [crad]	0.099	4.3×10^{-5}	0.096
		$u_A(\bar{\varphi}_u)$	4.1×10^{-5}	2.7×10^{-4}	5.6×10^{-5}
100	Ratio error	$\bar{\varepsilon}_u$ [%]	-2.1×10^{-4}	3.5×10^{-4}	-4.2×10^{-4}
		$u_A(\bar{\varepsilon}_u)$	1.2×10^{-4}	1.7×10^{-4}	1.1×10^{-4}
	Phase displacement	$\bar{\varphi}_u$ [crad]	0.099	0.098	0.097
		$u_A(\bar{\varphi}_u)$	2.2×10^{-5}	3.5×10^{-5}	3.2×10^{-5}
120	Ratio error	$\bar{\varepsilon}_u$ [%]	-0.005	-0.005	-0.002
		$u_A(\bar{\varepsilon}_u)$	1.1×10^{-4}	1.2×10^{-4}	2.1×10^{-4}
	Phase displacement	$\bar{\varphi}_u$ [crad]	0.100	0.098	0.097
		$u_A(\bar{\varphi}_u)$	2.4×10^{-5}	3.1×10^{-5}	2.5×10^{-5}

Another test is performed in order to characterize the amplitude response of the voltage divider at rated frequency. In this case, the actual primary voltage is specified to be 2%U_P, 5%U_P, 25%U_P, 50%U_P, 80%U_P, 100%U_P, 120%U_P, 150%U_P, 200%U_P, and 250%U_P. For each input voltage, 20 repetitive

measurements are performed in order to obtain the average ratio error and phase displacement, which are then presented in Fig. 9 (a) and (b). The positive and negative limits of accuracy class 0.5P are also reproduced for comparison [6]. As clearly demonstrated in Fig. 9 (a) and (b), the performances of the capacitive voltage divider are fully compliant with the 0.5P accuracy class constrains for primary input voltage ranging from 2% to 250% of the rated voltage. In the range from 80% and 120% of the rated voltage, the device fulfills also the requirement of the 0.2 accuracy class for measuring LPVT. Furthermore, the average values and the evaluated Type-A uncertainties are listed in TABLE III, validating the stability of the measurement results.

TABLE III. Mean values and Type-A standard uncertainties of ratio error and phase displacement of the voltage divider at 50Hz.

Percentage of U_P [%]	Ratio error		Phase displacement	
	$\overline{\varepsilon_u}$ [%]	$u_A(\overline{\varepsilon_u})$	$\overline{\varphi_u}$ [crad]	$u_A(\overline{\varphi_u})$
2	-0.68	2.3×10^{-3}	0.101	1.8×10^{-3}
5	-0.097	1.4×10^{-2}	0.092	8.8×10^{-4}
25	-0.061	2.8×10^{-4}	0.094	1.2×10^{-4}
50	-0.046	1.8×10^{-4}	0.094	3.1×10^{-4}
80	-0.014	1.1×10^{-4}	0.097	6.5×10^{-5}
100	-0.0005	2.4×10^{-4}	0.097	4.3×10^{-5}
120	-0.005	1.7×10^{-4}	0.098	3.5×10^{-5}
150	-0.005	1.4×10^{-4}	0.098	3.8×10^{-5}
200	-0.0025	1.3×10^{-4}	0.098	8.4×10^{-5}
250	0.00079	1.9×10^{-4}	0.095	9.8×10^{-5}

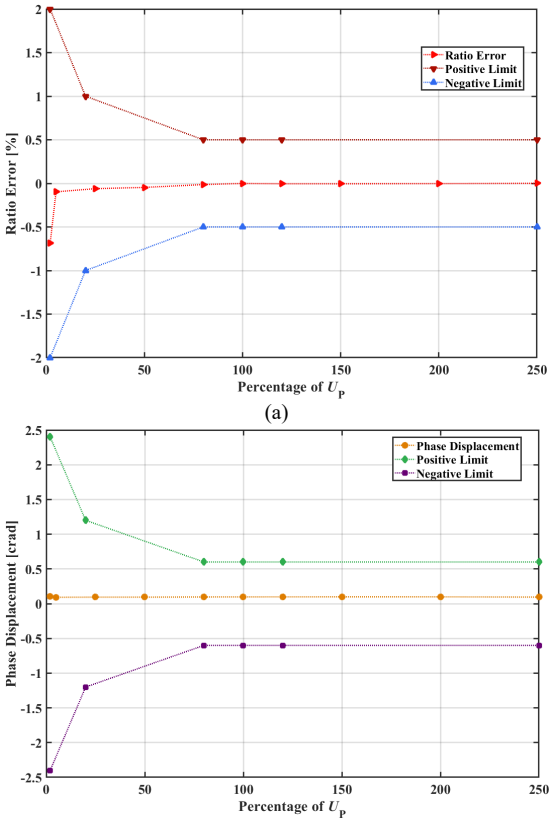

Fig. 9. (a) Ratio error and (b) phase displacement versus the percentage of the rated primary input of the capacitive voltage divider.

In addition to the basic accuracy test made in accordance with the standard, test for accuracy versus harmonic frequency is conducted. From a practical point of view, this test is carried out with a single harmonic frequency applied at the primary voltage for each measurement. For such purpose, harmonics from the 2nd up to the 100th order are measured at each actual primary input 25%U_P, 50%U_P, 80%U_P, 100%U_P, 120%U_P, 150%U_P, 200%U_P, and 250%U_P. The experimental results in terms of the ratio error and phase displacement are shown in Fig. 10 (a) and (b). Good harmonic responses are obtained, which clearly confirm that the capacitive voltage divider complies with the accuracy requirements on harmonics [8].

To characterize the impact of the temperature variation on the behavior of the capacitive voltage divider, the temperature dependent accuracy test is carried out. The considered ambient temperature points are 25°C, 30°C, 40°C, 50°C, 55°C, and 60°C. The rated primary voltage with frequency ranging from 49.5Hz, 50Hz, 50.5Hz and up to the maximum 5000Hz is applied. The ratio error and phase displacement are reproduced in Fig. 11 (a) and (b), respectively.

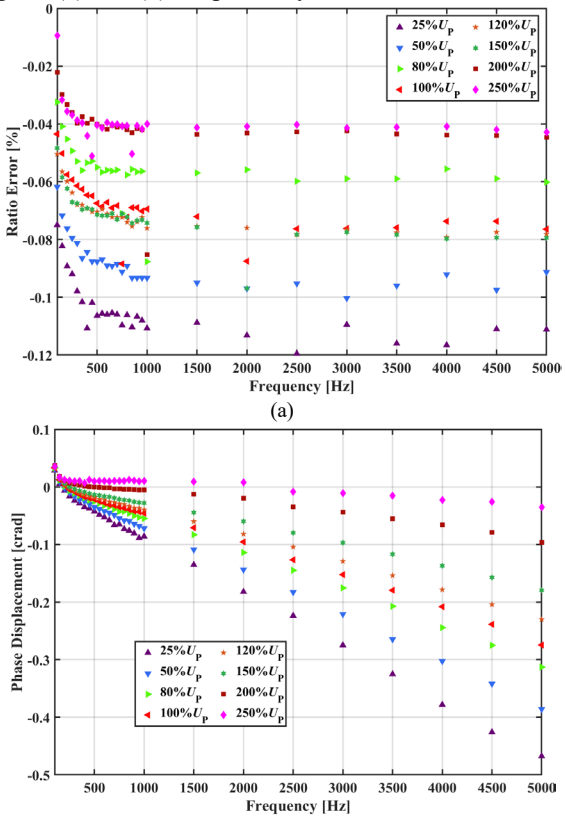

Fig. 10. Accuracy assessment for harmonic response to the capacitive voltage divider: (a) ratio error and (b) phase displacement.

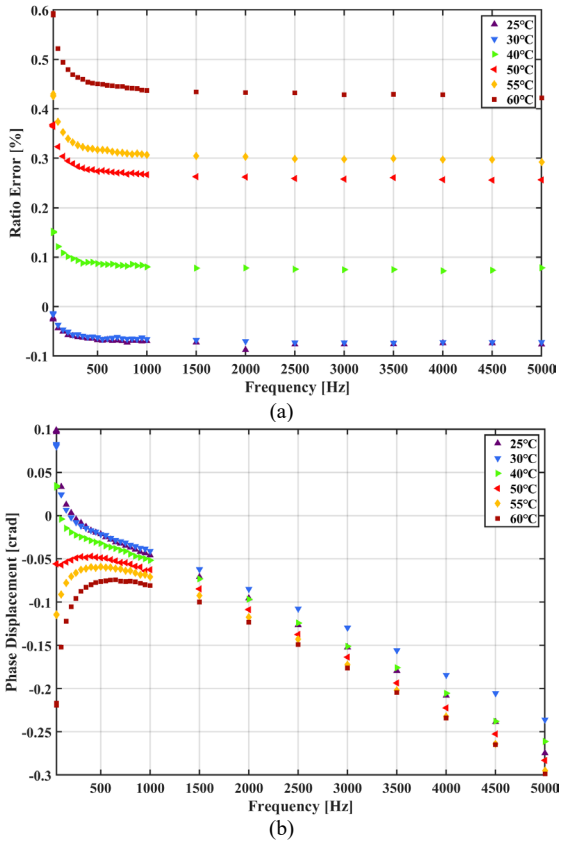

Fig. 11. (a) Ratio error and (b) phase displacement at the rated primary voltage under temperature dependent test.

As can be identified, the ratio error increases as the temperature rises. This behavior can be due to the presence of thermal drift of the employed resin material, although it has been carefully selected. Remark that a critical issue arises to the ratio error at 60°C when the frequency is lower than 200Hz. In this frequency range, the ratio error is beyond the limit of accuracy class 0.5, with a maximum value 0.59%. Even at the extreme case of 60°C, the phase displacement is quite low. As for the rest of the temperature points, both ratio error and phase displacement are within the constraints of accuracy class 0.5.

C. Characterization of the Shielded RC Based Current Transformer of the Combined LPIT Prototype

In this subsection, accuracy tests are applied to the current channel of the combined LPIT prototype for the purpose of characterization study.

As a first test, a basic measuring accuracy test to the RC based current transformer is performed by using the schematic in Fig. 7. A test current at rated frequency 50Hz with amplitude percentages of the rated primary current has been used. For each actual primary current, 10 tests are performed for the purpose of evaluating the mean values and the Type-A uncertainties of ratio error and phase displacement. Fig. 12 (a) and (b) show the average values of ratio error and phase displacement versus the percentages of rated primary current, respectively. The ratio error and phase displacement limits under the measuring accuracy class 0.1 as defined in the standard [7] are illustrated ranging from 5% I_P to 120% I_P. Additionally, the constraints from 1% I_P to 5% I_P are given under the requirement of accuracy class 0.2S for special applications.

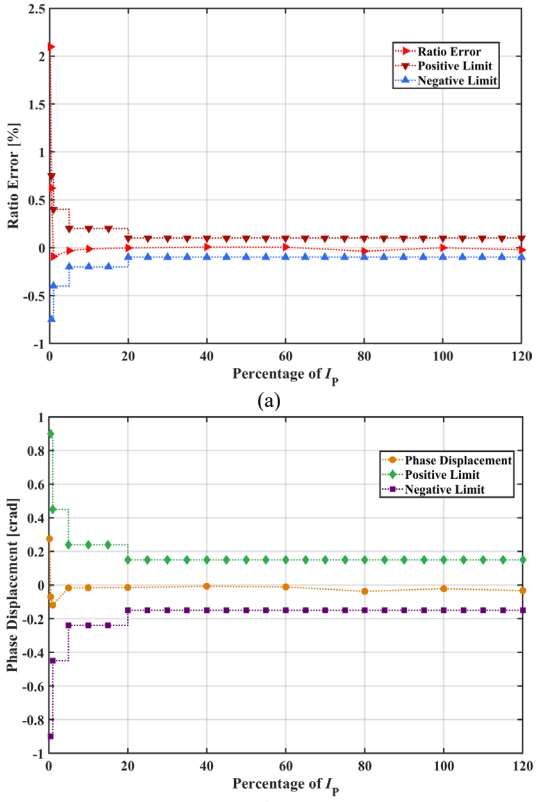

Fig. 12. (a) Ratio error and (b) phase displacement versus the percentage of rated primary current of the RC based current transformer.

As shown in Table IV, type A uncertainty is never greater than one tenth of the value of uncertainty B (due the current reference). Consequently, we can assume that the overall uncertainty of the current transformer is such that it falls within the accuracy classes 0.1 and 0.2S.

TABLE IV. Type-A standard uncertainties of ratio error and phase displacement of the Current Transformer at 50Hz.

Percentage of I_P [%]	Ratio error	Phase displacement
	$u_A(\overline{\varepsilon}_i)$	$u_A(\overline{\varphi}_i)$
0.2	1.9×10^{-2}	1.5×10^{-3}
0.5	5.7×10^{-4}	4.4×10^{-4}
1	1.0×10^{-4}	6.7×10^{-5}
5	8.7×10^{-5}	1.2×10^{-5}
10	3.7×10^{-5}	1.3×10^{-5}
20	3.4×10^{-5}	1.2×10^{-4}
40	3.3×10^{-5}	1.9×10^{-5}
60	3.3×10^{-4}	1.6×10^{-5}
80	2.9×10^{-5}	1.7×10^{-5}
100	5.0×10^{-6}	9.3×10^{-6}
120	4.0×10^{-5}	1.5×10^{-5}

In general, current harmonics can be generated in electrical systems due to the adoption of specific non-linear devices. In order to characterize the frequency response of the current transformer, another basic accuracy test is performed. For such purpose, frequency band ranges from the rated frequency up to the 50th order with a uniform step of 50Hz is applied. Remark that to avoid the measurement circuit clipping issues, the tests at harmonics are carried out under the condition that the primary input current magnitude reduces in proportion with the

increasing of harmonic frequency. The measurement results considering the ratio error and phase displacement are presented in Fig. 13 (a) and (b), respectively. The constraints of the ratio error and phase displacement up to the 50th harmonic of accuracy class 0.1 is reproduced. As can be noted, the frequency responses of the ratio error and phase displacement remain within the requirements of accuracy class 0.1, indicating good performances at high frequencies from the standard point of view.

Due to practical limitations, the temperature dependent accuracy test cannot be performed at rated current by using the circuit diagram described in Fig. 7. As a consequence, an alternative solution is adopted, as indicated in Fig. 6. The calibrator is used to generate a primary current with a constant amplitude of 20A and harmonic frequency ranging from the 2nd to the 100th order. This specific test is carried out at specified ambient temperatures from 25℃, 30℃, 40℃, 50℃, to 60℃. The ratio error and phase displacement versus frequency and temperature are illustrated in Fig. 14 (a) and (b), respectively. As expected, bigger ratio error is obtained at 60℃ with a maximum value -0.38% at 5000Hz, due to the thermal drift behavior of the RC unit. On the contrary, the phase displacement behavior of the RC is less sensitive to the temperature drift, although it increases as the frequency increases, as demonstrated in Fig. 14 (b). The test results on the RC based current transformer confirm that it is basically suitable for quality measurements up to the 100th order harmonic even at the extreme case at 60℃.

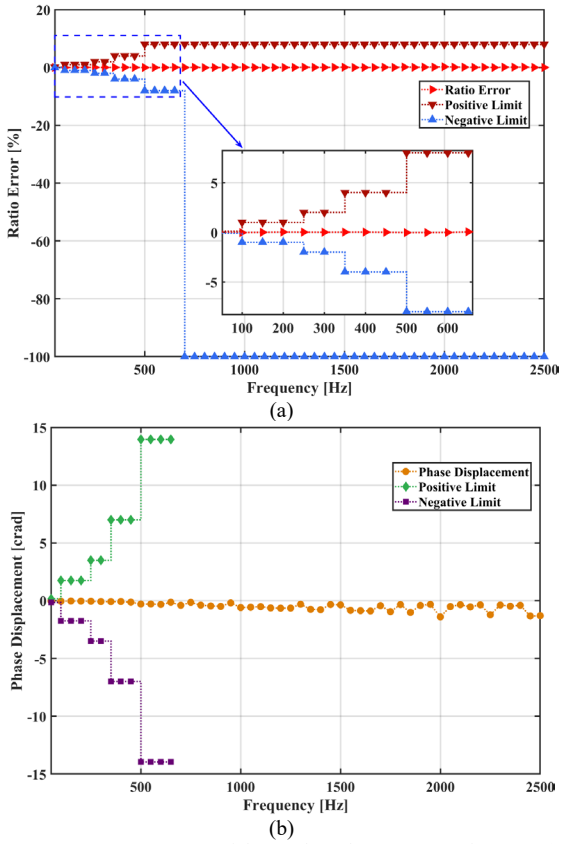

Fig. 13. Frequency responses of the RC based current transformer: (a) ratio error and (b) phase displacement.

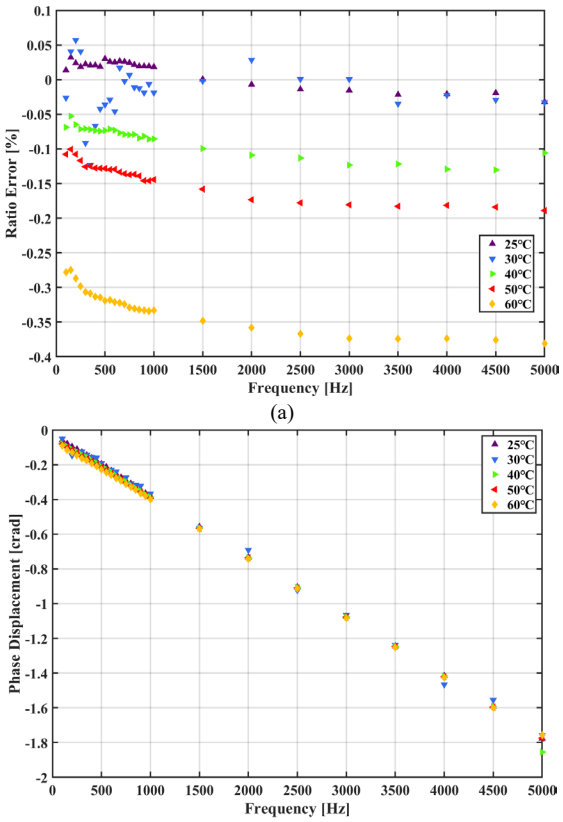

Fig. 14. Temperature cycle accuracy test for the RC based current transformer at primary current 20A: (a) ratio error and (b) phase displacement.

V. Conclusion

In this paper, a novel design of combined voltage and current LPIT for low voltage applications is proposed. It is basically composed of a shielded RC for current measurement and a capacitive divider for voltage transduction. The proposed solution exploits the RC shield as an electrode for the high voltage capacitance of the voltage divider. Fundamental principles have been presented, demonstrating the effectiveness of the proposed combined LPIT scheme. A prototype has been developed and characterized. Measurement results on the combined LPIT prototype confirm that the accuracy both on voltage and current channels can be expected up to the 100th order harmonic. A particular point that should be emphasized is that to achieve high precision at extreme temperatures a resin material and a shielded RC scheme with low thermal drift is mandatory. Nevertheless, remarkable features of the proposed combined LPIT have been verified and consequently it is deemed to have considerable applications in low voltage smart substations. An interesting development is design and construction of a combined transducer for LV applications, but with a current range of 60A, reducing its dimensions as much as possible and integrating the electronics inside the screen box. In this way we would have a device that could find a very wide application. Moreover, the design and characterization of a three-phase combined LPIT will be investigated in the future work.

REFERENCES

[1] A. Mingotti, C. Betti, L. Peretto, and R. Tinarelli, "Low-Power Instrument Transformers and Energy Meters: Opportunities and Obstacles," *IEEE Instrumentation & Measurement Magazine*, vol. 26, no. 4, pp. 44-48, 2023.

[2] G. Crotti, G. D'Avanzo, P. Letizia, and M. Luiso, "The Use of Voltage Transformers for the Measurement of Power System Subharmonics in Compliance with International Standards," *IEEE Trans. Instrum. Meas*., vol. 71, Article Sequence Number: 9005912, 2022.

[3] M. Normandeau and J. Mahseredjian, "Evaluation of Low-Power Instrument Transformers for Generator Differential Protection," *IEEE Trans. Power Del.*, vol. 33, no. 3, pp. 1143-1152, Jun. 2018.

[4] G. Crotti, D. Gallo, D. Giordano, C. Landi, and M. Luiso, "Medium Voltage Divider Coupled with an Analog Optical Transmission System," *IEEE Trans. Instrum. Meas*., vol. 63, no. 10, pp. 2349-2357, 2014.

[5] H. Miroslav, J. Radek, and P. Vaclav, "Low-power Instrument Transformers Frequency Response and Accuracy Requirements for Harmonics," in *Proc. 25th International Conference and Exhibition on Electricity Distribution*, Madrid, Spain, 3-6 June 2019, pp. 1-5.

[6] *Instrument Transformers—Part 11: Additional Requirements for Low-Power Passive Voltage Transformers*, IEC 61869-11:2018.

[7] *Instrument Transformers—Part 10: Additional Requirements for Low-Power Passive Current Transformers*, IEC 61869-10:2018.

[8] *Instrument Transformers—Part 1: General Requirements*, IEC 61869-1:2023.

[9] T. Yamada, K. Tachibana, and T. Shioda, "Design method for a wideband resistive voltage divider based on average impedance matching with optimal solution methods," *IEEE Trans. Instrum. Meas*., vol. 70, pp. 1-7, 2021.

[10] B. Li, Y. He, L. Wang, M. Cao, Z. Fu, and H. Zhang, "Calibration method of a wideband AC resistance voltage divider based on an equivalent model," *Sensors*, vol. 23, pp. 1-13, 2023.

[11] E. Mohns, C. Jiang, H. Badura, and P. Raether, "A fundamental step-up method for standard voltage transformers based on an active capacitive high-voltage divider," *IEEE Trans. Instrum. Meas*., vol. 68, no. 6, pp. 2121-2128, Jun. 2019.

[12] A. Ghaderi, A. Mingotti, L. Peretto, and R. Tinarelli, "Low-Power Voltage Transformer Smart Frequency Modeling and Output Prediction up to 2.5 kHz, Using Sinc-Response Approach," *Sensors*, vol. 20, no. 17, pp. 1-20, 2020.

[13] Q. Xu, C. Dong, and Y. Huang, "An Electronic Voltage Transducer Based on Electrostatic Charge Escape," *IEEE Trans. Instrum. Meas*., vol. 71, pp.1-8, 2022.

[14] W. Wu, Y. Xu, X. Xiao, and H. Hu, "Research on Proximity Effect in Measuring Error of Active Electronic Voltage Transformers," *IEEE Trans. Instrum. Meas*., vol. 65, no. 1, pp.78-87, Jan. 2016.

[15] A. Mingotti, F. Costa, G. Pasini, L. Peretto, and R, Tinarelli, "Modeling Capacitive Low-Power Voltage Transformer Behavior over Temperature and Frequency," *Sensors*, vol. 21, no. 5, pp. 1-19, 2021.

[16] A. Mingotti, L. Peretto, and R. Tinarelli, "Novel and Simplified Procedure to Test Immunity of Low-Power Voltage Transformers," *Sensors*, 2022, 22, 5804.

[17] A. Brandolini, M. Faifer, and R. Ottoboni, "A Simple Method for the Calibration of Traditional and Electronic Measurement Current and Voltage Transformers," *IEEE Trans. Instrum. Meas*., vol.58, no. 5, pp. 1345-1353, May. 2009.

[18] A. Mingotti, L. Peretto, R. Tinarelli, and K. Yigit, "Simplified Approach to Evaluate the Combined Uncertainty in Measurement Instruments for Power Systems," *IEEE Trans. Instrum. Meas*., vol. 66, no. 9, pp. 2258-2265, Sep. 2017.

[19] K. Stankovic and U. Kovacevic, "Combined measuring uncertainty of capacitive divider with concentrated capacitance on high-voltage scale," *IEEE Trans. Plasma Sci*. vol. 46, no. 8, pp. 2972-2978, 2018.

[20] P. Pegoraro, K. Brady, P. Castello, C. Muscas, and A. von Meier, "Compensation of systematic measurement errors in a PMU-based monitoring system for electric distribution grids," *IEEE Trans. Instrum. Meas*., vol. 68, no. 10, pp. 3871-3882, Oct. 2019.

[21] A. Mingotti, A. Baldi, L. Peretto, and R. Tinarelli, "A General Easy-to-Use Expression for Uncertainty Evaluation in Residual Voltage Measurement," *IEEE Trans. Instrum. Meas*., vol. 69, no. 4, pp. 1576-1584, Apr. 2020.

[22] W. Rogowski and W. Steinhaus, "Die messung der magnetischen spannung," *Elect. Eng.*, vol. 1, no. 4, pp. 141-150, 1912.

[23] S. Ziegler, R. C. Woodward, H. H. C. Iu, and L. J. Borle, "Current sensing techniques: A review," *IEEE Sensors J.*, vol. 9, no. 4, pp. 354-376, Apr. 2009.

[24] M. H. Samimi, A. Mahari, M. A. Farahnakian, and H. Mohseni, "The Rogowski coil principles and applications: A review," *IEEE Sensors J.*, vol. 15, no. 2, pp. 651-658, Feb. 2015.

[25] M. Marracci, B. Tellini, C. Zappacosta, and G. Robles, "Critical Parameters for Mutual Inductance Between Rogowski Coil and Primary Conductor," *IEEE Trans. Instrum. Meas*., vol. 60, no. 2, pp. 625-632, Feb. 2011.

[26] X. Liu, H. Huang, and C. Jiao, "Modeling and Analyzing the Mutual Inductance of Rogowski Coils of Arbitrary Skeleton," *Sensors*, vol. 19, no. 15, pp. 1-16, 2019.

[27] A. Mingotti, L. Peretto, and R. Tinarelli, "Effect of the Conductor Positioning on Low-Power Current Transformers: Inputs for the Next IEC 61869-10," *Electricity*, vol. 2, no. 1, pp. 1-12, 2021.

[28] A. Mingotti, L. Peretto, and R. Tinarelli, "Effects of Multiple Influence Quantities on Rogowski-Coil-Type Current Transformers," *IEEE Trans. Instrum. Meas*., vol. 69, no. 7, pp. 4827-4834, Jul. 2020.

[29] Y. Xu, X. Zou, and X. Wang, "Influencing Factors and Error Analysis of Pulse Current Measurement with Air-Core Rogowski Coil," *IEEE Trans. Plasma Sci*., vol. 48, no. 12, pp. 4381-4386, Dec. 2020.

[30] K. Draxler and R. Styblikova, "Magnetic shielding of Rogowski coils," *IEEE Trans. Instrum. Meas.*, vol. 67, no. 5, pp. 1207-1213, May 2018.

[31] B. Ayhan and C. Ucak, "Improved Magnetic Circuit Model for Magnetic Shielding Effectiveness in Rogowski Coil," *IEEE Trans. Mags.* vol. 56, no. 3, Article Sequence Number: 8500109, pp. 1-9, Mar. 2020.

[32] T. Tao, Z. Zhao, W. Ma, Q. Pan, and A. Hu, "Design of PCB Rogowski coil and analysis of anti-interference property," *IEEE Trans. Electromagn. Compat*., vol. 58, no. 2, pp. 344-355, Apr. 2016.

[33] Q. Chen, H. Li, and B.-X. Huang, "An innovative combined electronic instrument transformer applied in high voltage lines," *Measurement*, vol. 43, no. 7, pp. 960-965, 2010.

[34] M. Faifer, S. Toscani, and R. Ottoboni, "Electronic combined transformer for power-quality measurements in high-voltage systems," *IEEE Trans. Instrum. Meas*., vol. 60, no. 6, pp. 2007-2013, Jun. 2011.

[35] E. Lesniewska and J. Olak, "Improvement of the Insulation System of Unconventional Combined Instrument Transformer Using 3-D Electric-Field Analysis," *IEEE Trans. Power Del*., vol. 33, no. 6, pp. 2582-2589, Dec. 2018.

[36] B. Lu, W. Huang, J. Xiong, B. Su, and Z. Liu, "Study on a new power frequency capacitive voltage transducer for gas insulated substations based on capacitive voltage division," *IEEE Trans. Instrum. Meas*., vol. 70, pp.1-9, 2021.

[37] B. Lu, W. Huang, J. Xiong, L. Song, Z. Zhang, and Q. Dong, "The study on a new method for detecting corona discharge in gas insulated switchgear," *IEEE Trans. Instrum. Meas*., vol. 71, pp. 1-8, 2022.

[38] M. Olguin, C. Yanez, F. Cortes, and E. Ramirez, "Electric stress grading on bushings of combined instrument transformers using high permittivity polymeric composites," *IEEE Trans. Dielectr. Electr. Insul.*, vol. 20, no. 6, pp. 2335-2342, Dec. 2013.

Youpeng Huangfu (Member, IEEE) received the B.Sc. degree in electrical engineering from Jilin University, Changchun, China, in 2012, and the Ph.D. degrees in electrical engineering from the Politecnico di Milano, Milan, Italy, and Xi'an Jiaotong University, Xi'an, China, in 2019. From October 2019 to October 2023, he was a Research Associate with the Department of Electronics, Information and Bioengineering, Politecnico di Milano, Milan, Italy.

Since November 2023, he has been a Professor at the School of Electrical Engineering, Xi'an Jiaotong University, Xi'an, China. His current research interests include the

characterization of instrument transformers, electromagnetic compatibility, and arc fault detection for electrical systems.

Marco Faifer (Senior Member, IEEE) was born in Bormio, Italy, in 1978. He received the Laurea degree in electronic engineering and the Ph.D. degree in electrical engineering from the Politecnico di Milano, Milan, Italy, in 2003 and 2009, respectively.

He is currently an Associate Professor with the Dipartimento di Elettronica, Informazione e Bioingegneria, Politecnico di Milano. His scientific activity is mainly concerned with DSP techniques and the development of industrial sensors and devices for high-voltage measurements. Moreover, he develops measurement algorithms for the characterization of electrical components and materials. He also works in the field of diagnostics for electrical devices.

Roberto Ottoboni (Fellow, IEEE) received the Laurea and Ph.D. degrees from the Politecnico di Milano, Milan, Italy, in 1987 and 1992, respectively. From January 2009 to December 2012, he was the Chair of the Electrical Engineering Department, Politecnico di Milano.

He is currently a Full Professor of electrical and electronic measurements with the Dipartimento di Elettronica, Informazione e Bioingegneria, Politecnico di Milano. His research interests include the range from the study and analysis of digital signal processing techniques for measurement to the study and implementation of sensors, transducers, and measurement systems for electrical quantities for industrial applications, with particular attention to innovative sensors for medium, and high voltages and high currents.

Sergio Toscani (Senior Member, IEEE) received the M.Sc. and Ph.D. degrees (summa cum laude) in electrical engineering from the Politecnico di Milano, Italy, in 2007 and 2011, respectively.

From 2011 to 2020, he was an Assistant Professor in electrical and electronic measurement with the Dipartimento di Elettronica, Informazione e Bioingegneria, Politecnico di Milano, where he is currently working as an Associate Professor. His research interests include the development and testing of current and voltage transducers, measurement techniques for power systems, electrical components, and systems diagnostics.

Prof. Toscani is a member of the IEEE Instrumentation and Measurement Society and the IEEE TC-39-Measurements in Power Systems.